EuroVis 2018
R. S. Laramee, G. E. Marai, and M. Sedlmair
(Guest Editors)

Volume 37 (2018), Number 3
STAR – State of The Art Report

Survey of Cardiovascular Visualization Techniques

Christian Brändle and Niko Leopold

TU Vienna

Abstract

The visualization of cardiovascular structures is an essential aspect of the diagnostic process therapy planning. This survey provides an overview over recent advances in both model-free and model-based vascular visualization techniques. In the field of direct volume rendering, the focus is on advanced transfer function design to highlight abnormalities of the vessel wall, as well as providing aggregated rotation independent 2D projections and depth cues for effective diagnosis. Furthermore, improved model-based techniques are discussed, which provide more accurate and effective sceletonization and surface reconstruction.

Categories and Subject Descriptors (according to ACM CCS): I.3.3 [Computer Graphics]: Picture/Image Generation—; 1.3.7 [Computer Graphics]: Three-dimensional Graphics and Realism—; 1.3.5 [Computer Graphics]: Computational Geometry and Object Modeling—;

Keywords: Cardiovascular visualization, direct volume rendering, raytracing, transfer function design, intensity projection, curviplanar reformation, geometric modeling, vascular system modeling, convolution surfaces, implicit modeling, vessel reconstruction method, level sets, quad dominant meshes

1. Introduction

For diagnosis as well as for therapy planning it is crucial to understand the branching pattern and morphology of tree-like anatomical structures [PB13]. Depending on the capturing technique we are confronted with 3D data that could have very high spacial or temporal resolution. The visual analysis of this static or dynamic data is a challenging task.

Figure 1: *Medical visualization pipeline.*

The medical visualization pipeline shown in figure 1 serves as orientation how vascular structures are visualized. We are focusing on 3D image processing and visualization. The interested reader will find a complete survey of the whole pipeline for instance in [PB13].

Our goal here is to describe recent methods to visualize vascular structures. Our initial interest is on how to separate these structures from background data. Direct volume rendering techniques can be used to visualize this enhanced and visually separated data. If a more concrete separation is necessary, surface visualization techniques may be preferable, which involve segmentation and centerline extraction.

Visualization techniques are spilt into *model-based* and *model-free* approaches. Model-based mesh generation follows some more restrictive assumptions about the vascular structure whereas model-free methods such as direct volume rendering tries to capture as much original information as possible. Model-based techniques are often used for treatment planning and basic anatomical overview, whereas model-free methods are required for precise diagnostics.

2. Direct Visualization

Model-based techniques are based on assumptions that limit their applicability to certain real world applications. Especially in diagnostic settings, where simplifying assumptions are not acceptable, it is essential to visualize the data directly äs it is". Direct Volume Rendering via GPU ray tracing, together with filtering and projection techniques is primarily employed for this purpose.

Volume Data is typically acquired via X-ray or magnetic resonance tomographic imaging techniques (CT, MR). To segment the vascular structures from the other tissue, so called "vesselness"filters that preserve only tubular structures can be used. A high vesselness for example may be defined as a situation where one of the three eigenvalues of the Hessian matrix (matrix of second derivatives) is considerably larger than the other two, indicating variance in one main direction. Other vesselness filter additionally employ entropy based filtering. Other tubular structures, like bones, are not reliable removed via such methods, however. In the case of angiography (CTA, MRA), i.e. the visualization of the vessels, an

intravenous contrast agent is typically used. However, the intensities of structures enhanced via the contrast agent are often similar to the high intensitites resulting from bony structures. Thus, bones are typically removed via semi-automatic (where the user clicks at a structure) or automatic methods that involve region growing.

One of the main diagnostic tasks where DVR is employed is the detection of pathological conditions in vasculature, such as stenosis (narrowing of the vessel wall) or aneurisms (balloon-like bulges in the vessel wall) as well as obstructions from plaques or blood clots. An essential aspect in this regard is the choice of the transfer function, that maps intensity values sampled along rays in tracing to color and opacity values. Typically in DVR, these color and opacitiy values are accumulated, such that the contributions of occluded regions might not make it into the final image, since full opacity is already reached earler on the ray thus leaving to chance of the intensities farther away to reach the eye. Thus for example, in a 3D visualization the detection of pathological conditions that are surrounded by a lot of other tissue, may be difficult due to such occlusion.

Specialized Transfer Functions for 3D Views

To provide a means of inspecting dense volumetric data in a 3D view more easily, intensity projection techniques are used. The most widely known technique in this context is Maximum Intensity Projection (MIP), which simply means that the maximum of all intesities sampled along a ray is assigned to its corresponding pixel. MIP allows for distant high-intensity structures, such as calcified plaques or stents, to ßhine through"from arbitrary distances without being influenced by lower intensity tissues along the ray. Other projection techniques are Minimum Intensity Projection (MINIP), which may reveal soft plaques. Soft plaques consisting mainly of lipids are separated from the vessel lumen only by a thin fibrous cap, which is prone to rupture; blood clot formation around the rupture can lead to blocking of the artery. Average Intensity Projection is less commonly employed.

Notably, there is one important limitation of these intensity projection techniques: There is a loss of depth information of the projected intensity values, as the accumulation of color and opacity along the ray is not given as in DVR. The user is thus required to rotate the view to get a proper understanding of the spatial structure via motion parallax. Closest Vessel Projection, also known as Local MIP, uses the first local maximum in intensity above a user defined threshold. Thus, vessels of high intensity that are closer than the global maximum can be visualized as well, while low intensity structures still have no influence.

A more recent approach in the design of transfer functions, by Bruckner and Gröller [BG09] combines the advantages both traditional DVR (depth perception via occlusion from opacity accumulation) as well as MIP (highlighting structures of high intensity even though they are occluded by structures of lower intensity). Their technique is called Maximum Intensity Difference Accumulation. The idea is to adjust the blending factor used in the accumulation of samples along the ray based on the change in the maximum intensity samples so far. As long as the maximum intensity is unchanged from previous samples, the last sample contributes fully with its opacity and color like in DVR. However if the intensity of the next sample is a new maximum, then the previous value (i.e. all that was accumulated before) is weighted less, leaving more opacity for the new maximum intensity to shine through, as seen in Figure 2. Thus there is an accumulation, but local maxima are highlighted as well. Using a single control parameter, the user can

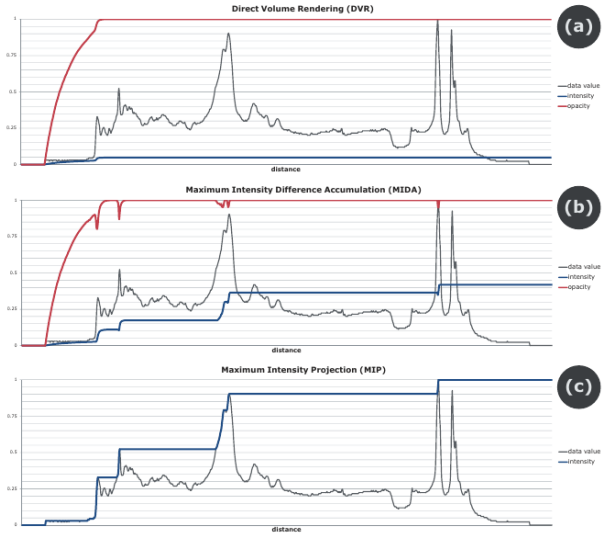

Figure 2: *Ray profiles for DVR, MIDA and MIP.*

switch between more accumulation (more like DVR) or more emphasis of maxima (more like MIP), as seen in Figure 3. MIDA thus presents a unifying method of both traditional DVR and MIP via a simple extension. Bruckner and Gröller also enhance the technique with gradient based shading, a common technique used in DVR, and weight the contribution of the shading by the magnitude of the gradient to avoid noise in homogenous regions.

While MIDA proves very useful for the visualization of vascular structures, it is still a very general technique. Other techniques are tailored more towards specific diagnostic tasks, such as the visual emphasis of pathological structures. Glasser et al. [GOH*10] present a method that aids the quantitative evaluation of coronary artery plaque via specialized transfer functions that are automatically adjusted to fit the segmented artery data. Specifically, their approach aims to emphasize the vessel wall and its abnormalities, like hard and soft plaques or stents. Initially, a segmentation of the coronary arteries is performed. Then, the mean and standard deviation of both blood and vessel wall are computed. This is however not as straightforward as it may seem, due to non-uniform contrast agent accumulation and differing Hounsfield (HU) units. To overcome this limitation, the authors compute an intensity profile volume (IPV) for each artery branch. Each IPV is a stack of histograms computed radially from vessel centerline positions in its orthogonal planes, as seen in Figure 4. These histograms are then used to determine the local mean and standard deviations for blood and vessel wall. The transfer function is designed in a way such that both the vessel wall and soft plaques as well as high intensity structures such as hard plaques are highlighted, as seen in Figure 5. The

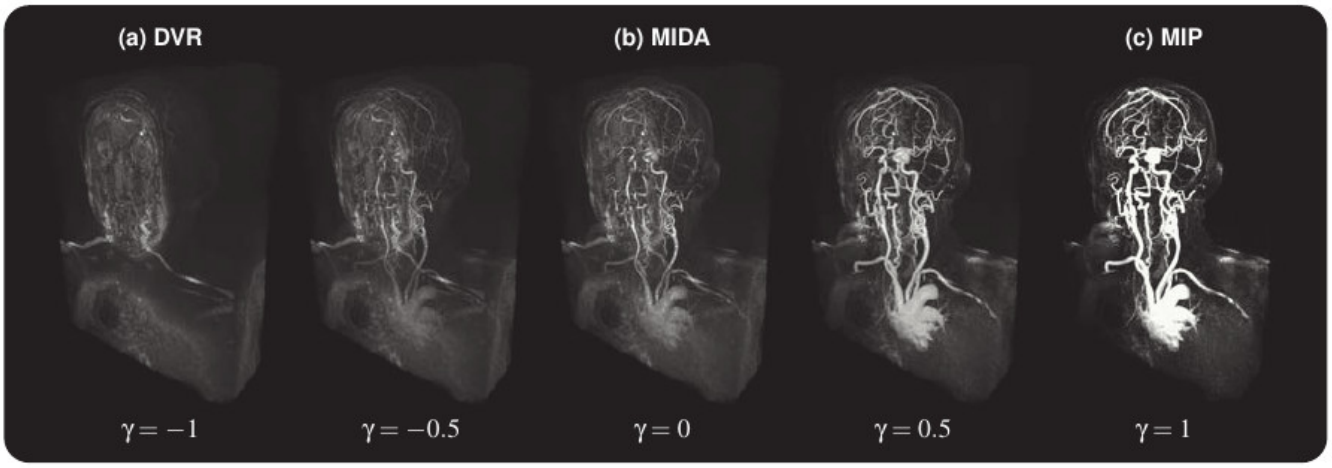

Figure 3: *Maximum Intensity Difference Accumulation provides a technique that unifies both traditional DVR and MIP. Using a single control parameter, the user can switch between more accumulation (more like DVR) or more emphasis of maxima (more like MIP).*

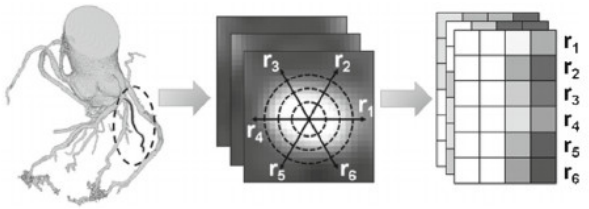

Figure 4: *Computation of Intensity Profile Volumes to determine local blood and vessel wall intensity distribution of each branch.*

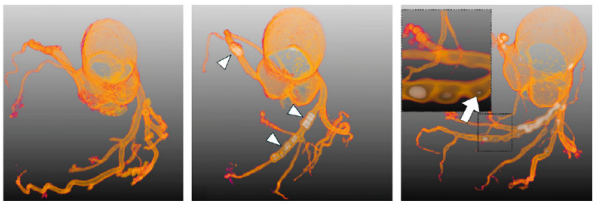

Figure 6: *Results of the automatically adjusted transfer functions by Glasser et al. [GOH*10] to highlight vessel wall and abnormalities such as plaques or stents.*

tresholds are set automatically corresponding to the computed local branch intensity distributions. Two thresholds, S_3 and S_6 can be adjusted by the user, determining the average vessel wall intensity and the threshold for hard plaque. Results can be seen in Figure 6.

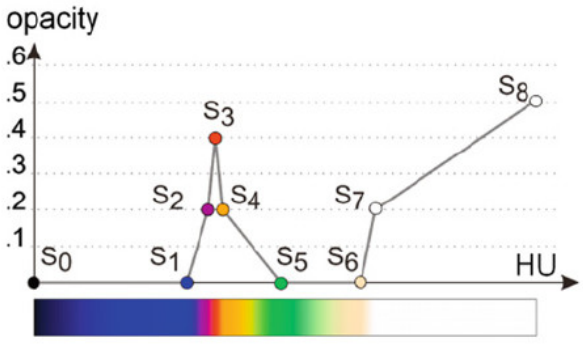

Figure 5: *A transfer function that highlights vessel wall and hard plaques, automatically adjusted to local intensity distribution.*

Rotation Independent Projection Techniques for 2D Views

When it comes to the inspection of volumetric data via 2D views, other projection techniques are used, to ensure visibility of possibly occluded vascular structures. A widely used technique is Curved Planar Reformation (CPR), of which the basic three types are projection CPR, stretched CPR and straightened CPR. Two more recent improvements to CPR are discussed in the following.

Mistelbauer et al. [Mis10] present a technique called Centerline Reformations (CR), that aims at simultaneously visualizing the inside (lumen) of multiple arbitrarily oriented vessels in CPR. Using CPR, the vessel lumen may be inspected by defining a curved cut along the vessel centerline. However this is only possible for single vessels, not for the whole vessel tree. In CR, first the vessel centerlines and radii are extracted from the volume via scale-space feature detection: Contrast-enhanced data is filtered using a Hessian-based vesselness filter followed by a segmentation based on Hysteresis thresholding as used by the Canny edge detector. The Hysteresis thresholding uses two threshold values to ensure continuous edges without gaps, when the data fluctuates: When the data is below the lower threshold, it is rejected, but if it is inbetween the thresholds, it is still accepted if it is connected to a value above the higher threshold. The union of the resulting binary volumes is then used

to determine the radius via the Hessian scale with maximum response, and the centerlines are extracted using skeletonization via a thinning technique. Then, a graph representation of the vessel tree is additionally computed to allow for user interaction such as selection etc. The vessel lumen itself is then rendered using wavefront propagation from the vessel centerline, which is based on the Fast Marching Method (FMM). The initial wavefronts are simply arrays of pixels along the centerline from orthogonal projection of the volume to the 2D view. For each pixel additional data is stored: the corresponding graph edge, voxel, pixel type (vessel, halo, background) vessel radius as well as the depth and arc-length (distance of pixel in projected space to the first pixel of the centerline). The wavefronts (arrays of pixel data) are then propagated to neighboring pixels orthogonal to the centerline until the radius is reached assigning the corresponding projected volume data along the way, then optionally continuing by drawing a halo, as seen in Figure 7. For background pixels, traditional MIP or MIDA can be used. Since

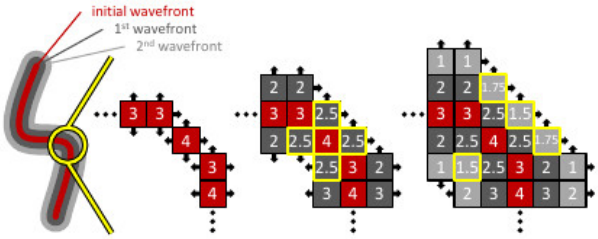

Figure 7: *Results of the automatically adjusted transfer functions by Glasser et al. [GOH*10] to highlight vessel wall and abnormalities such as plaques or stents.*

vessels may overlap, the wavefront propagation requires a comparison of the currently stored pixel buffer at closest depth with the current vessel wavefront. Since a wavefront may also collide with itself leading to ambiguities in value assignment, the arc length, i.e. position along the centerline of pixels is also propagated and used for this decision.

A different technique also presented by Mistelbauer et al. [MMV*13] is called Curvicircular Feature Aggregation (CFA). The idea of CFA is to reduce the amount of user interaction required when working with CPR angiography data, i.e. rotation around the vessel centerline to inspect it from all directions. CFA provides a single image where aggregated intensities around the vessel centerline are depicted. This is done by sampling intensities in circular rays around the assumed vessel centerline and aggregating the samples with MIP or MINIP, as shown in Figure 9. Samples may be placed along the circular rays either at costant angles or constant arc-lengths, the latter providing more samples and thus also more computational overhead. The resulting image is split in two parts: The centerline is straightened and placed vertically from top to bottom, separating the image in left and right side. Thus the vertical dimension relates to the position along the centerline. The horizontal distance from the centerline corresponds to the radius of the circular rays: Each pixel at certain horizontal distance from the centerline shows the result of the aggregation around a circular ray with the corresponding radius. On the left side, MIP is used for the aggregation (or rather, projection), on the right side MINIP is used. For radii that by far exceed the vessel radius, there is no point in

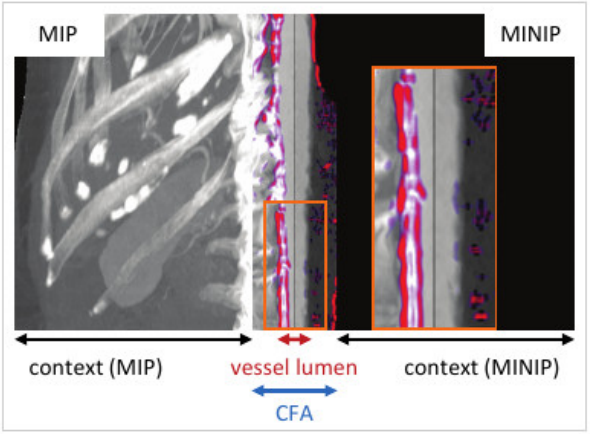

Figure 8:

doing the curvicircular feature aggregation. Instead, standard MIP and MINIP projections from a single direction are shown in pixels beyond a certain horizontal distance from the centerline, to use the image space for context, as seen in Figure 8. Another feature of the technique is to display a measure of stability of the centerline estimation at each given point along the vessel. This is done by computing the variance of values sampled in the neighborhood of each centerline point, to determine the local uniformity around it. If there is a high variance, i.e. low stability, the centerline estimation may deviate from the actual centerline in the vessel volume data. The variance is mapped to a color range from red to blue, red meaning higher variance, i.e. less stability.

Depth Cues for Direct Volume Rendering

Kersten-Oertel et al. [KOCC14] provide an extensive evaluation of monoscopic depth cues used in real time renderings of 3D angiographic data. The fast and accurate perception of relative depth and structure of overlapping vessels is essential for intraoperative guidance, where surgeons often have little time to make important decisions. The study compares the effectiveness of fog (mapping of depth to saturation), pseudo-chromadepth (mapping depth to color from red to blue), kinetic depth (depth by continuous rotation around the structure), edges as well as stereopsis (using shutter glasses).

The authors note a number of limitations of the operating room. Interaction with the data (which can provide depth cues via the parallax effect apparent from the movement) are typically not possible due to the need for sterility. The surgeon typically needs to verbally instruct an assistant to do the interaction via mouse and keyboard, thus making real time interaction unfeasable. Moreover, head mounted displays to provide stereopsis are typically not acceptable due to operating room constraints. Thus monoscopic depth cues play an important role.

The study shows results of experiments where participants had to state which of two vessels is closer, for each of the depth cues

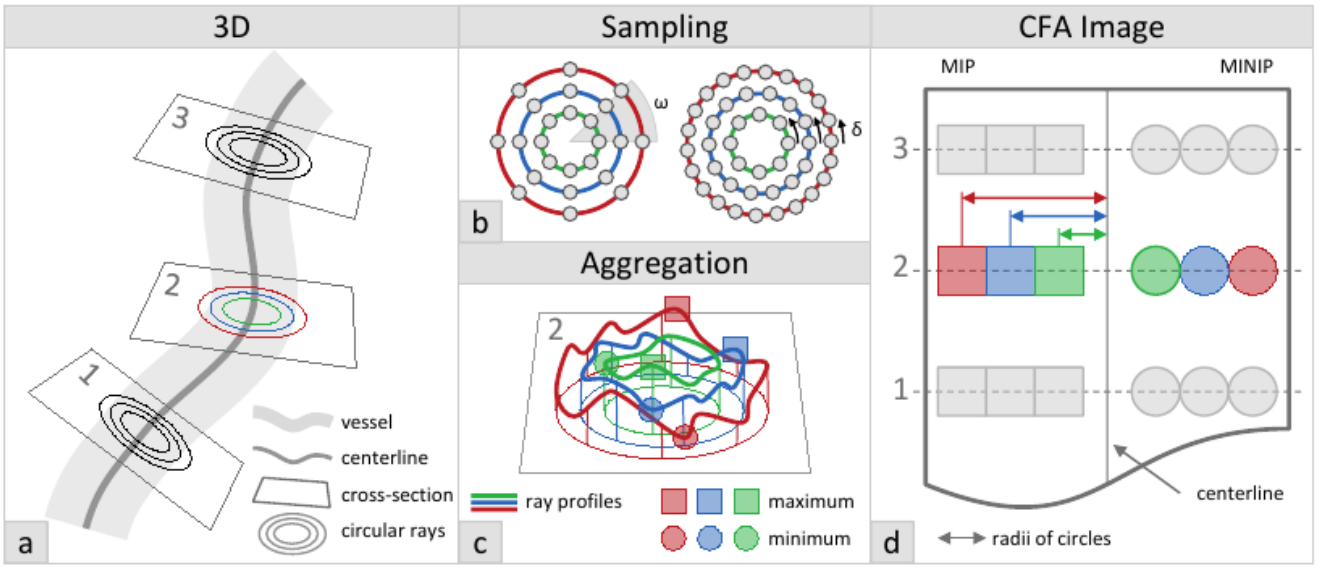

Figure 9:

and with all possibly influencing parameters randomized. In results both with novices unexperienced in vasculature as well as expert neurosurgeons, both the fog and pseudo-chromadepth cues gave best results both in time and correctness. Accordint to the authors, the short time needed to provide the correct result indicates that little additional processing is required, reducing the perception of depth to a comparison of saturation or hue. The kinetic depth cue proved unreliable and prone to confusion of front and back due to orthographic projection used in clinical settings. The stereoscopic cue interestingly did not yield better results, indicating that their benefit is task dependent. The edge cue was beneficial for expert neurosurgeons, who used the edge information to trace the path of vessels to determine which was closer.

3. Skeletonization

Skeletonization can be seen either as integral part of surface visualization techniques or as an separate preprocessing step. Actually both is true according to the observed methods as some surface visualization techniques compute the skeleton in an internal stage of the process. Here we focus on the preprocessing step. Skeletonization here is actually a reduction of dimension on the segmentation data. We actually reduce the volumetric segmentation data or two dimensional surface data to a one dimensional graph structure. Nevertheless the graph itself is embedded in a 3D space. The skeleton itself is a compact representation of 2D or 3D shapes that preserves many of the topological and size characteristics [A*02]. Bium et al. [Biu64] provides a common definition of the skeleton as the locus of centers of maximal discs (or spheres) contained in the original object.

There are actually three ways of generating skeletons and medial axes. The first one is *morphological thinning* there the boundary of an object is peeled off layer by layer till those points remain which removal would cause topological change [A*02]. As this is based on heuristics and is not based on the maximal discs approach this is the weakest of the skeletonization techniques, though the easiest one. The second is based on *Voronoi diagrams* where the diagram represent the boundary's medial axis [A*02]. While the most accurate one, this technique is also the most complex and expensive one. The third way is based on *distance transforms* of oebject's boundaries [A*02]. Here Sethian et al. [Set96] proposed the *Fast Marching Method* (FFM) for evolution of boundaries in normal direction where the skeleton lies along the singularites. However the detection of those singularities is difficult and possibly unstable.

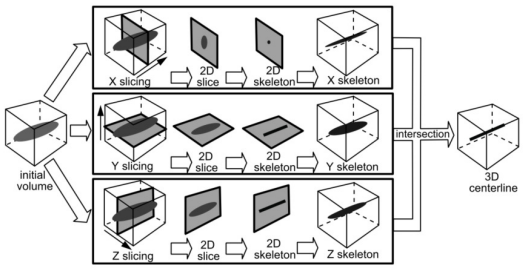

Figure 10: *Centerline computation pipeline.*

[A*02]

Telea et al. [A*02] augment the Fast Machring Method by computing the parametrized boundary location every pixel came from. The resulting prameter field is thresholded to produce the skeleton branches. As his initial attemt focus on 2D problems he did an extension on 3D that utilize three distance transforms on the corresponding axis-parallel planes and intersect the resulting volumes to get a 3D centerline on the object as shown in figure 10.

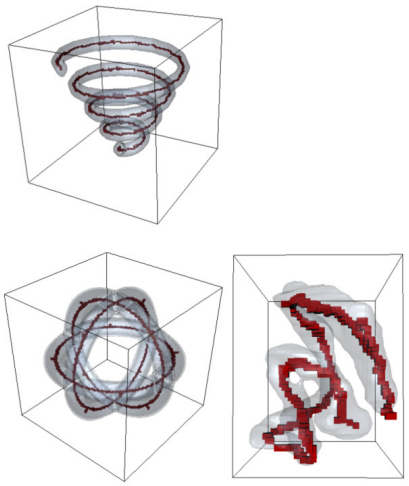

Figure 11: *Examples of 3D centerlines.*

[A*02]

As this approach do only respect the maximum distance from the boundary in the three orthogonal slice planes it is only an approximation. The real centerline would be at the location where centers of boundary-touching spheres are positioned. But for real world data the difference do not seem to be of big impact as shown in figure 11.

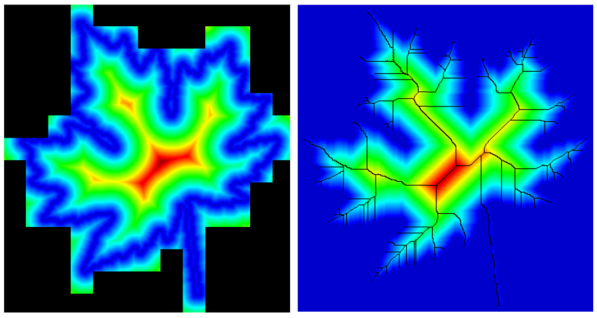

Figure 12: *Tiling and skeleton of a leaf.*

[ST04]

Strzodka et al. [ST04] further accelerates the generation of the 2D skeleton using graphics hardware. Based on the concept of *footprint splatting* the combination of different spalts produces a weighted distance transform in real time. *Distance splatting* uses OpenGL fragments to propagate signals in the *feature distance transform* (FDT). The FDT follows the previously described concept that skeletons are defined as the set of centers of maximal balls contained in the boundary of the observed object. Tiling of the original object further speeds up the process. Results are pixel-level correct skeletons for all boundaries and thresholds, as shown in figure 12.

4. Surface visualization techniques

In this section we will focus on different surface visualization techniques. Roughly we can divide surface mesh generation into *model-based* and *model-free*.

The model-based mesh generation makes some assumptions about the model, in our case about the vascular system. In peculiar it makes assumptions about the topological structure, the observed junctions and the profiles of vessels. The topological structure is mostly represented by a graph and limited to a tree like representation. Also the observed junctions often are limited to certain kinds of junctions like bifurcations. Finally the profiles of the vessels are simplified to circular or elliptical structures. All this simplifications and assumptions can help to speed up the process of surface generation, to make it more reliable or more visually pleasing or even transform the underlying data into more usable data for further processing. The downside is that model-based meshes do not resemble the underlying data as accurate as it could be done and also sometimes simplify the underlying data too much such that essential features are lost. Especially when diagnoses of vascular degenerations or similar detail based inspections need to be done model-based approaches may not provide enough vivid information of the underlying data.

Here model-free mesh generation comes into play. The goal here is to retain as much of the underlying data as possible. But without a underlying model the extraction and creation of the mesh is more time consuming and cumbersome. Moreover unwanted results can arise if the underlying data suffers from noise or other failures in capturing. So care must be taken at the decision what for data is extracted and finally represented in the resulting mesh.

From the literature observed we determined that most of the methods require at some points a skeletonization of the underlying data. For now we assume that the underlying data consists of a voxel model that represents a density field of captured values. As model-based methods require a model, all of the observed methods require an extraction of a skeleton prior to the actual mesh generation. In regards of skeletonization the interested reader is reffered to Ebert et al. [EBN02] or Strzodka et al. [ST04].

As seen model-based mesh generation is based more or less on geometrical assumptions and reasoning on the model. Volkau et al. [VZB*05] for instance models a cerebral arterial model from segmented and skeletonized angiographic data. He constructs a vascular structure consisting of tube segments and bifurcations, so this model-based approach limits the domain of representable data quite hard in regards of branching possibilites. The centerline is smoothed with a sliding average filter to prevent problems with outliers and the two kinds of topologies, namely tubular and B-Subdivison based ones, are combined to form the complete vessel structure.

A connected graph is established that captures also the blood flow direction. This is done by splitting it up into two connected tree structures where one is designated as inflow structure. The model shapes the tube segments with decreasing radius with respect to the bloodflow as well as it captures radii change at bifurcations. This is based on statistical data. Radii at bifurcations are approximated with an exponential function whereas radii evolution at tubular parts are done via linear regression. At connection points C1 con-

tinuity is established via further constraints. So no abnormal cross section shape or diameter will show up easily in the final result.

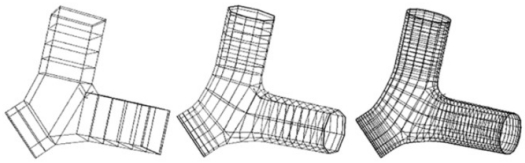

Figure 13: *Example of refinement with B-subdivision.*

[VZB*05]

The bifurcations themselves are constructed based on B-subdivison. The generation of quadrangles of a bifurcation till the overlapping internal part is shown in figure 13. Internal parts are subdivided to fit the outer subdivison. Problems with this scheme arise when all three vessels at the bifurcation form a close to orthogonal connection, where the inner face will be undefined. Also the B-subdivision of tubular segments show problems, namely self intersections when the radius of of curvature is smaller than the radius of the tube, shown in figure 14. Further problems mentioned are 'oversampling' or unrealistic sampling of bifurcations according to a too coarse sample pattern or problems with centerline smoothing in very jaggy areas as an acceptable smoothing also will remove esential features of the underlying vascular structure.

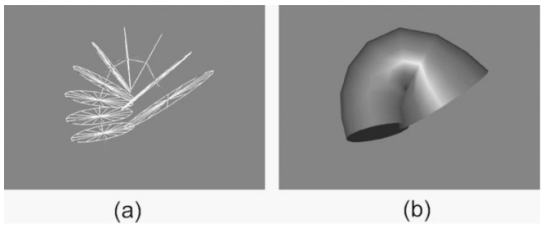

Figure 14: *Fold of vessel when curvature is higher than tube radius.*

[VZB*05]

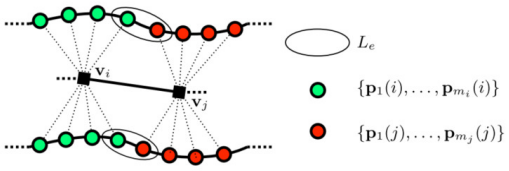

Figure 15: *Estimation of thickness of graph edges.*

[SEEK12]

Another geometry based modelling approach is provided by Sibbing et al. [SEEK12]. His work is focusing on quad meshes as they are visually more pleasant, require fewer elements and can produce more stable results in further processing, like FEM. Here the topologically correct extraction of the branching structure is done from a post-processed triangle mesh that is generated from an adapted *Marching Cubes* algorithm based on the interior voxels which are identified via a variant of the *Level Set* method. The extracted mesh is shrinked to a close to one dimensional structure that serves as basis for a tree based graph as well as for radius estimation along its edges, see figure 15. Further the graph is used to subdivide the triangle mesh into tubular parts and parts with one or more furcations with appropriate placed cutting planes. The so called *interfaces* are 2D polygons between adjacent segments. They are defined by the intersection of cutting planes with the triangular mesh.

Quad meshes for the junctions are created with the *Mixed Integer Quadrangulation* by Bommes et al. [BZK09]. The quads are just required to align with the defined boundary to generate radially arranged quads.

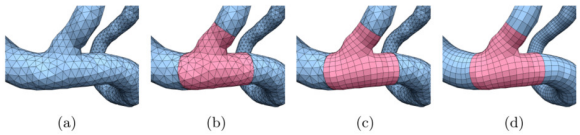

Figure 16: *(a) The input to our remeshing stage is a smoothed and resampled version of the mesh extracted using the Marching Cubes Algorithm. (b) The mesh is partitioned into junction and tube components. The cuts insert additional vertices at the respective interfaces. (c) We remesh the junctions yielding a fair quad layout. (d) Tubes are remeshed, such that the final mesh is a quad dominant mesh.*

[SEEK12]

Tubes now only have to provide a smooth transition between two interfaces with a possibly different number of vertices. The rings of the tubes are generated out of equidistant iso-contours on the harmonic scalar field on the tube. Triangles are introduced between so called transition rings to compensate for the difference in vertices. The distribution of the transition rings as well as the distribution of the triangles around the tube in a transition case is done via adaption of the Bresenham line rasterization algorithm. Stretching of quads along the tube axis as well as rotations of the rings to get configurations with almost 90 degree angles in the quads, yields close to optimal quad dominant meshes. The advantage of this reconstruction is the smoothing of unwanted artifacts on the original triangle mesh as well as the already shown properties of quad meshes, see figure 16.

Figure 17: *Transition at branching.*

[OP05]

A technique that uses the vessel skeleton as input data but only

respects the diameter information at the provided graph is called *convolution surfaces*. The main idea is that *implicit surfaces* describe the original surface by equations to model smooth, deformable objects. Oeltze et al. [OP05] used a combination of so called 'blobs' to model an *iso-surface* out of this scalar field function. The resulting convolution surface is a surface of an object around its skeleton. The convolution itself is done on an integral of 'blob-functions' along the skeleton. It is actually the modification of a signal by a filter, in this case a Gaussian filter. To speed up the process filter functions with finite support are used and the scalar field is only computed within certain bounding volumes around the line segments. Unwanted blending at branchings is avoided by more narrow filter kernels, see figure 17. Blending between segments that are close but not connected is avoided by restricted support on the skeleton, see figure 18.

Figure 18: *Unwanted blending.*

[OP05]

Still the problems of convolution surfaces are that they only support a circular base shape at tubes, that unwanted bulging can be suppressed but not completely removed and that unwanted blending of close parts is still possible. Finally the end segments have always the shape of a half sphere which neither represents the normally open ends of vascular trees nor has low deviation from the original surface in that areas.

In contrast model-free mesh generation mostly rely on some implicit functions that should resemble the input data instead of explicit constructive reasoning in geometric elements like tubes and junctions. Also here there are different techniques that respect the original shape more or less. Convolution surfaces therefore form a bridge between model-based and model-free mesh generation as the technique already use an implicit function but limit the shape in a model-based fashion.

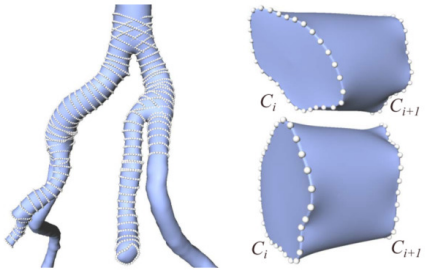

Figure 19: *Reconstruction of an arterial tree from free-form contours.*

[KBT*12]

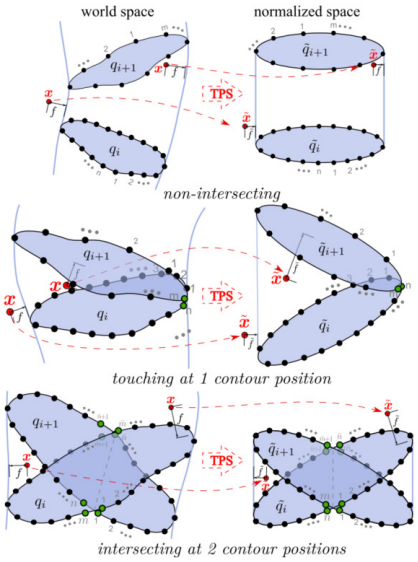

Figure 20: *Mapping of neighboring free-form contour pairs to normalized shapes.*

[KBT*12]

To capture vascular profiles and open endings of vascular structures Kretschmer et al. [KBT*12] uses an adaptive modelling with non circular cross sections. He generates intersection-free surfaces from centerlines with complex outlines, see fituge 19. He decomposes the centerline description into segments which are locally described by implicit functions and combines them using boolean operations. In this fashion all intersection- and furcation-related issues are solved in similar fashion to convolution surfaces with the difference that the capturing of the vascular outline is not so limited. A watertight scale-adaptive mesh is generated out of an adaptive octree in the end. The key difference to CS is that the so called *admissible distance functions* (ADFs) just form a class of functions with the property to detect valid iso-surfaces. To find a topology-preserving mapping that forms a intersection free surface part between two adjacent contours on the vascular structure found by the ADFs they follow the idea of *thin plate splines*. The assignment of contour pairs to a limited set of target shapes guarantee a valid surface topology when the contours do not touch, touch or penetrate each other as shown in figure 20.

The octree that should capture also the smallest vessels is recursivly subdivided at surface intersections with the grid. To speed up queries on the octree a localized approximation of the implicit function with a certain threshold to safely prune cells is used. To improve the quality of the extracted mesh a bisection method is used to interpolate between values when marching cubes is applied, advantages of this scheme is shown in figure 21.

Finally Wu et al. [WWL*10] also generates scale-adaptive surfaces from vascular structures with similar properties. He extracts the vascular boundary voxels from the segmentation and use them to build a 3D point cloud where normals are estimated via covariance analysis. Then a 3D implicit indicator function os compu-

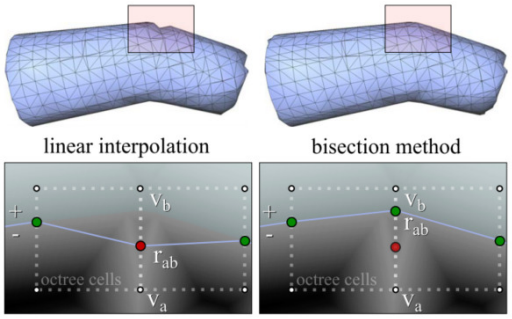

Figure 21: *Improved root-finding of the iso-surface using bisection method.*

[KBT*12]

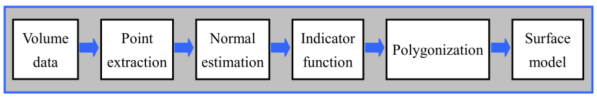

Figure 22: *Pipeline of geometric modeling of vascular tree structures.*

[WWL*10]

ted from the point cloud ba solving a Poisson equation. Finally the surface is generated by adaptive polygonization. The surface is a smooth, morphologically topology correct two-manifold that is scale-apdaptive to the local curvature ans have fewer and better shaped triangles compared to earlier approaches. The pipeline used is shown in figure 22.

To reconstruct very thin vessel structures an adaptive point extraction is used that relies on the constellation of adjacent object voxels. Normals are estimated on k-nearest neighbours of a point in the point cloud and the smallest eigenvalue of their covariance matrix. The implicit function that approximates the surface of the point samples is a Poisson surface reconstruction. It utilize the vector field and generates a function gradient best approximates the normal field of the point cloud.

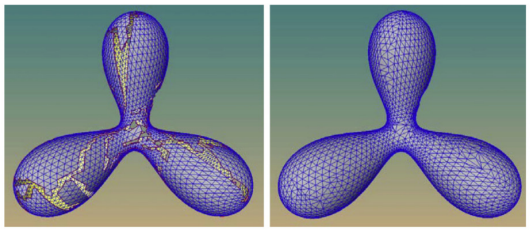

Figure 23: *Polygonization of a trifurcate model. A long gap is produced upon the termination of mesh expanding stage (left), and is sewed in the subsequent gap-stitching stage (right).*

[WWL*10]

The polygonization is done by an advancing front algorithm utilizing Newton step method. Care has been taken to ensure that the

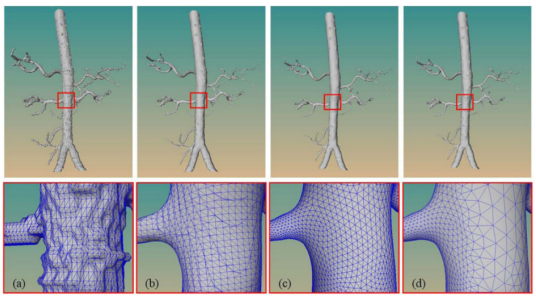

Figure 24: *Comparison of triangle quality for an aorta tree. Surface model generated by the marching cubes (a), multi-level partition unity based method (b), subdivison surface based method (c) and sclae-adaptive surface method (d). The bottom row is a zoomed region corresponding to the rectangle region of the top row.*

[WWL*10]

minimal angle of triangles is maximized in the triangulation step. The resulting gap on the surface is then closed via a stitching operation, see figure 23. Also here the patching triangles are subdivided to a similar size than the surrounding ones. To further refine and smooth the mesh a Loop based subdivison is performed. A comparison of several methods is shown in figure 24. It can be seen that the scale-adaptive nature of the reconstructed mesh together with the smooth and but still good approximation of the underlying shape yields very good results on vascular structures.

4.1. Conclusions

We have reviewed some recent techniques in the field of direct and indirect (model-free and model-based) visualization of vascular structures.

Regarding model-free techniques the focus was on improvements to the traditional direct volume rendering methodology. Specifically, improvements to the design of transfer functions were presented, that provide both depth information as well as highlighting high intensity structures such as contrast-enhanced vessels or vessel abnormalities. An essential usability feature is the provision of transfer functions that require little or no user interaction while still providing good results for arbitrary data. Regarding projections to 2D views, improvements to traditional Curved Planar Reformation have been presented that remove the need of rotating around a vessel by aggregating intensities to provide a rotation independent overview.

With regard to the indirect surface visualization techniques we saw that the proper choice of a method depends heavily on the intended use case. For educational visualization sometimes simple model-based visualizations are preferred as they remove unnecessary or abnormal data and focus on the statistical average model to provide the basic overview to students. In clinical diagnosis however, every abnormal detail of a blood vessel is likely of high interest, meaning that model-free approaches are often required as they more closely represent the actual data. Also, potential subsequent use of the generated models, such as in fluid simulations, may in-

fluence the selected methodology, e.g. to have quad based patches instead of triangular ones for mesh description.

To conclude, we should emphasize that the choice of the visualization method should be motivated primarily by the application requirements. The field of vascular visualization is still evolving and provides numerous research challenges, especially in the automatization of visualization techniques for arbitrary data, especially for detection of pathological conditions, the combination of both context and detail rendering, as well as uncertainty visualization in diagnostic settings. An interesting topic of research would also be the tracking of surgical instruments during an operation and their visualization in the context of direct volume rendering.

References

[A*02] ALEXANDRU T., ET AL.: An augmented fast marching method for computing skeletons and centerlines. 5, 6

[BG09] BRUCKNER S., GRÖLLER M. E.: Instant volume visualization using maximum intensity difference accumulation. In *Computer Graphics Forum* (2009), vol. 28, Wiley Online Library, pp. 775–782. 2

[Biu64] BIUM H.: A transformation for extracting new descriptions of shape. In *Symposium on Modeis for the Perception of Speech and Visua1 Form* (1964). 5

[BZK09] BOMMES D., ZIMMER H., KOBBELT L.: Mixed-integer quadrangulation. *ACM Transactions On Graphics (TOG) 28*, 3 (2009), 77. 7

[EBN02] EBERT D., BRUNET P., NAVAZO I.: An augmented fast marching method for computing skeletons and centerlines. 6

[GOH*10] GLASSER S., OELTZE S., HENNEMUTH A., KUBISCH C., MAHNKEN A., WILHELMSEN S., PREIM B.: Automatic transfer function specification for visual emphasis of coronary artery plaque. In *Computer Graphics Forum* (2010), vol. 29, Wiley Online Library, pp. 191–201. 2, 3, 4

[KBT*12] KRETSCHMER J., BECK T., TIETJEN C., PREIM B., STAMMINGER M.: Reliable adaptive modelling of vascular structures with non-circular cross-sections. In *Computer Graphics Forum* (2012), vol. 31, Wiley Online Library, pp. 1055–1064. 8, 9

[KOCC14] KERSTEN-OERTEL M., CHEN S. J.-S., COLLINS D. L.: An evaluation of depth enhancing perceptual cues for vascular volume visualization in neurosurgery. *IEEE transactions on visualization and computer graphics 20*, 3 (2014), 391–403. 4

[Mis10] MISTELBAUER G.: *Automated processing and visualization of vessel trees*. Citeseer, 2010. 3

[MMV*13] MISTELBAUER G., MORAR A., VARCHOLA A., SCHERNTHANER R., BACLIJA I., KÖCHL A., KANITSAR A., BRUCKNER S., GRÖLLER E.: Vessel visualization using curvicircular feature aggregation. In *Computer Graphics Forum* (2013), vol. 32, Wiley Online Library, pp. 231–240. 4

[OP05] OELTZE S., PREIM B.: Visualization of vasculature with convolution surfaces: Method, validation and evaluation. *IEEE transactions on medical imaging 24*, 4 (2005), 540–548. 7, 8

[PB13] PREIM B., BOTHA C. P.: *Visual computing for medicine: theory, algorithms, and applications*. Newnes, 2013. 1

[SEEK12] SIBBING D., EBKE H.-C., ESSER K. I., KOBBELT L.: Topology aware quad dominant meshing for vascular structures. In *Workshop on Mesh Processing in Medical Image Analysis* (2012), Springer, pp. 147–158. 7

[Set96] SETHIAN J. A.: A fast marching level set method for monotonically advancing fronts. *Proceedings of the National Academy of Sciences 93*, 4 (1996), 1591–1595. 5

[ST04] STRZODKA R., TELEA A.: Generalized distance transforms and skeletons in graphics hardware. In *Proceedings of the Sixth Joint Eurographics-IEEE TCVG conference on Visualization* (2004), Eurographics Association, pp. 221–230. 6

[VZB*05] VOLKAU I., ZHENG W., BAIMOURATOV R., AZIZ A., NOWINSKI W. L.: Geometric modeling of the human normal cerebral arterial system. *IEEE transactions on medical imaging 24*, 4 (2005), 529–539. 6, 7

[WWL*10] WU J., WEI M., LI Y., MA X., JIA F., HU Q.: Scale-adaptive surface modeling of vascular structures. *Biomedical engineering online 9*, 1 (2010), 75. 8, 9